Coordination of Modular Multilevel Converter based HVDC Terminals for Ancillary Services

Abel A. Taffese, Elisabetta Tedeschi
Dept. of Electric Power Engineering
Norwegian University of Science and Technology
Trondheim, Norway
abel.taffese@ntnu.no, elisabetta.tedeschi@ntnu.no

Abstract—This paper deals with the utilization of the energy storage capacity, inherently present in the Modular Multilevel Converter (MMC), in providing ancillary services to ac grids. The service considered in this paper is Power Oscillation Damping (POD), which requires active power injection and hence, causes distortion (oscillation) in the dc voltage. In a multi-terminal or meshed dc grid, the oscillation is compensated by active power taken from other terminal participating in dc voltage regulation. This action leads to propagation of the oscillation into other connected ac grids, which is undesirable. This can be avoided or reduced if the power injection is taken from the arm capacitors of the MMC. Such utilization of the MMC energy storage has already been proposed in literature. However, the amount of power that can be injected from one converter is very limited. Therefore, this paper proposes a method to coordinate such a functionality among multiple MMC terminals with the aim of obtaining higher capacity to accommodate more demanding services. Furthermore, communication between the terminals is not required because local measurement of the dc voltage is used as a feedback signal.

Index Terms—Modular Multilevel Converter, MMC, Energy Storage, Ancillary Services, Coordinated control

I. Introduction

An increasing number of grid codes are requiring HVDC converters to contribute more towards enhancing stability and power quality of the ac grid [1]. The contributions can be in the form of frequency regulation [2], Power Oscillation Damping (POD) [3], or ac voltage support to name a few. The first two services require manipulation of active power, which results in distortion on the dc voltage in the form of sags, swells, and oscillations. This causes converters terminals that participate in dc voltage regulation to provide the required active power in order to keep the dc voltage variations to a minimum. Thus, the voltage distortion by itself is not a major problem; it is the propagation of distorted active power that poses power quality challenges to the other connected ac grids. Another side-effect of this is that there is a strong dynamic coupling among the terminals, which can lead to negative interactions among multiple POD controllers acting on different ac grids, potentially reducing their performance [4]. Energy storage capacity inherently available in the HVDC converters, particularly the Modular Multilevel Converters (MMCs), can be used to mitigate this problem. It has been shown in literature [5], [6] that sub-module capacitors in the MMC can effectively provide the required power injection for the case of POD. Such schemes can also be extended to other type of services. There is, however, a limit on the amount power that can be obtained from the capacitors [6]. The limit is even lower for low frequency phenomenon like frequency regulation. This paper proposes a method that distributes the responsibility of providing energy storage among all the terminals connected to the dc grid. The methods proposed in [5], [6] are suitable for local compensation using a single converter, because they assume that the measurement of the power distortion is available. This requires communication of this signal in order to extend this scheme to multiple converters. The proposed method uses only local measurement of the dc voltage at each terminal, so it does not need communication. The main goal is to divert the power distortion into the arm capacitors of the converters. In doing so, the application of the method increases the apparent capacitance of the dc grid keeping the dc voltage variations to a minimum without drawing active power from the other ac grids. The energy based arm voltage control approach [7] is adopted in this paper. The remainder of this paper is organized as follows. First, the dynamic model of the converters with focus on average arm energy dynamics and dc voltage will be presented in Section II. Then, the control arrangement is discussed in Section III. The proposed approach is developed in Section IV, followed by simulation case studies in Section V. Finally, conclusions are presented in Section VI.

II. Modeling

This section presents a simplified average model of the MMC shown in Fig. 1. All the equations in this paper are in per-unit. The chosen per-unit convention will be presented first, followed by the average arm energy model.

A. Conversion to per-unit

The MMC dynamic equations contain components at multiple frequencies which can be grouped into dc and ac quantities. The quantities are grouped with the side they are closely related to. For example, the dc arm voltage is closely related to the dc side while the ac voltage is to the ac side. The complete list of the quantities together with their symbols and base values is given in Table I. Apparent power base value S_b
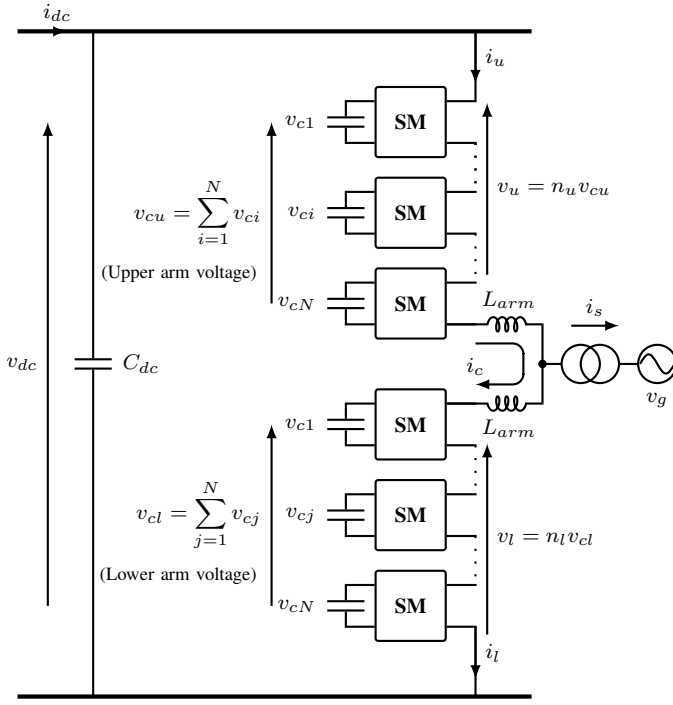
Figure 1: Per-phase circuit of the MMC.

TABLE I: Per-unit quantities with their base values

Symbol	Description	Per-unit base
v_{dc}	dc voltage	V_b^{dc}
i_{dc}	dc current	I_b^{dc}
i_c	per-phase circulating current	I_b^{dc}
$v_{cu/cl}$	arm voltage (sum of capacitor voltages)	V_b^{dc}
$i_{u/l}$	arm current	I_b^{dc}
c_p	arm capacitance (C_{arm}/C_b^{dc})	C_b^{dc}
l_{dc}	arm inductance (L_{arm}/Z_b^{dc})	Z_b^{dc}
r_{dc}	arm resistance (R_{arm}/Z_b^{dc})	Z_b^{dc}
v_s	ac phase voltage	V_b^{ac}
i_s	ac current	I_b^{ac}
l_{ac}	equivalent series ac inductance (L_{arm}/Z_b^{ac})	Z_b^{ac}
r_{ac}	equivalent series ac resistance (R_{arm}/Z_b^{ac})	Z_b^{ac}

is common to both sides. The resulting per-unit inductance and capacitance values have units in seconds, which correspond to the amount of time it takes their respective current and voltage to charge to the base value given that the base voltage and current are applied, respectively. The stored energy base value is chosen in such a way that the stored energy is equal to the square of the arm voltage in per-unit [7]. The base values are given in the Appendix.

B. Average arm energy model

Average model is selected because the focus in this paper is on active power balance. The most important assumptions made in the development of the model are:

- Lower level Sub-Module (SM) balancing control is ideal and the SM components are well-balanced. This enables aggregation of the SM capacitors into one equivalent arm capacitance.
- There is no ripple in the circulating current. This is reasonable because the ripple will be removed by using either compensated modulation [8] or circulating current suppression controllers [9].
- The number of SMs is large so that the insertion indexes are continuous.

The equations presented in this paper slightly differ from those in [7] because of the per-unit base values adopted. First, some basic definitions will be given. The upper and lower arm inserted voltages (v_u and v_l) are decomposed into common mode, v_c, and differential components, v_s, as shown in (1). The sign conventions and some variable definitions are shown in Fig. 1.

$$
\begin{aligned}
v_c &= \frac{1}{2}\left(v_u + v_l\right) \\
v_s &= \left(-v_u + v_l\right)
\end{aligned}
\tag{1}
$$

The same decomposition can be applied to the upper and lower arm currents (i_u and i_l) resulting in i_c and i_s as given by (2).

$$
\begin{aligned}
i_c &= \frac{1}{2}\left(i_u + i_l\right) \\
i_s &= \frac{3}{4}\left(i_u - i_l\right)
\end{aligned}
\tag{2}
$$

The differential components correspond to the ac side quantities. After applying this decomposition, the differential equation describing a simplified arm energy dynamics is given by (3).

$$
\begin{aligned}
\frac{\mathrm{d}}{\mathrm{d}t}w &= \frac{2}{c_p}\left[\frac{1}{2}\left(v_{dc}^* - 2v_c^*\right)i_c - \frac{1}{6}v_{sdq}^* \cdot i_{sdq}\right] \\
&\approx \frac{1}{c_p}\left[v_{dc}i_c - \frac{1}{3}\left(v_{sd}^* i_{sd} + v_{sq}^* i_{sq}\right)\right] \\
&= \frac{1}{3}\frac{1}{c_p}\left(p_{dc} - p_{ac}\right)
\end{aligned}
\tag{3}
$$

where w is the average arm energy, c_p is the per-unit arm equivalent capacitance, and i_c is the circulating current. v_{sdq}^* and i_{sdq} are the ac voltage reference and the ac current in dq domain, respectively. On the second line of (3), $(v_{dc}^* - 2v_c^*)i_c$ is substituted by $v_{dc}i_c$ by ignoring the dc side losses. Equation (3) shows that there will be a change in energy only when there is imbalance between the ac and dc side powers. Dynamics of i_c is captured by (4).

$$
\frac{\mathrm{d}}{\mathrm{d}t}i_c = \frac{1}{l_{dc}}\left(v_c^* - r_{dc}i_c\right)
\tag{4}
$$

where l_{dc} and r_{dc} are the arm inductance and resistance in per-unit to the dc base values. The dc link voltage is governed by the differential equation given in (5).

$$
\frac{\mathrm{d}}{\mathrm{d}t}v_{dc} = \frac{1}{c_{dc}}\left(i_{dc} - 3i_c\right)
\tag{5}
$$

where i_{dc} is the dc line current and c_{dc} is the equivalent dc side capacitance in per-unit. Finally, the ac current dynamics is given by (6) where ω is the fundamental frequency in $\mathrm{rad/s}$ and v_{gdq} is the grid voltage at the Point of Commom Coupling (PCC) in dq domain. l_{ac} and r_{ac} are the equivalent ac side inductance and resistance in per-unit to the ac base values.

$$\frac{\mathrm{d}}{\mathrm{d}t}i_{sdq} = \frac{1}{l_{ac}}\left(v_{sdq}^* - v_{gdq} - r_{ac}\mathbf{I}\cdot i_{sdq} - \omega l_{ac}\mathbf{J}\cdot i_{sdq}\right) \quad (6)$$
$$\mathbf{I} = \begin{bmatrix} 1 & 0 \\ 0 & 1 \end{bmatrix} \ and \ \mathbf{J} = \begin{bmatrix} 0 & -1 \\ 1 & 0 \end{bmatrix}$$

The next section discusses the control structure used in this paper.

III. CONTROL STRUCTURE

There are different controllers needed for proper operation of the MMC (Fig. 2). Here, active power and arm energy controllers are the main focus, so they will be discussed in subsequent sections.

A. Active power control

AC active power is controlled via the d-axis ac current which is in turn controlled by using the d-axis ac voltage reference, v_{sd}^*. Feedforward decoupling in the dq that is implemented in the current controller is not shown Fig. 2 for the sake of simplicity. DC voltage droop is added to the power reference if the converter is participating in voltage control. The droop constant ρ is usually in the range of few percent (e.g. 0.05 to 0.1) which means that a deviation in dc voltage causes 10 to 20 times larger deviation in active power in per-unit. All the controllers in Fig. 2 are tuned using modulus and symmetric optimum techniques [10].

B. Arm energy control

The arm energy is controlled via the circulating current, (Fig. 2). Power balance between the ac and dc sides is established by the energy controller. Any change in the ac active power appears as a disturbance to the energy controller (Fig. 2) and is rejected by adjusting the circulating current. Therefore, one can create a temporary difference between the ac and dc powers by adding a modification Δw to the energy reference w^*. This capability can be used to divert active power variations due to services such as POD into the arm capacitors. The main goal is to reduce the impact of a service given to one ac grid on another one in terms of active power distortion.

C. Relation between dc voltage and active power

A simplified relationship between dc voltage and ac active power will be derived in this sections. The result will be used in the development of the proposed controller in the next section. The analysis will focus on low frequency phenomena ($0.2\,\mathrm{Hz}$ to $2\,\mathrm{Hz}$) so all controllers in Fig. 2 can be assumed to be ideal. Hence, each controlled signal is set equal to

the respective reference value. Solving for i_c from (3), the following equation is obtained.

$$i_c = \frac{1}{v_{dc}}\left(c_p\frac{\mathrm{d}}{\mathrm{d}t}w + \frac{1}{3}p_{ac}\right) \quad (7)$$

p_{ac} can be substituted by the ac power reference including the droop as shown in (8).

$$i_c = \frac{1}{v_{dc}}\left[c_p\frac{\mathrm{d}}{\mathrm{d}t}w + \frac{1}{3}\left(p_{ac}^* - \frac{1}{\rho}\left(v_{dc}^* - v_{dc}\right)\right)\right] \quad (8)$$

The next step is to incorporate i_c into the dc link dynamic equation. For this purpose (5) will be extended to the case of a multi-terminal grid. If the resistance and inductance of the cables are ignored, the dc grid simplifies to one lumped capacitor. This is justified because the cable dynamics is much faster than the frequency of interest. This implies that the dc link voltage at each terminal is approximately the same and its dynamics is governed by (9)

$$c_g\frac{\mathrm{d}}{\mathrm{d}t}v_{dc} = -3\sum_{j=1}^{m}i_{cj} \quad (9)$$

where c_g is the equivalent grid capacitance and m is the number of converters. Substituting the values of i_{cj} from (8) yields,

$$c_g\frac{\mathrm{d}}{\mathrm{d}t}v_{dc} = -\sum_{j=1}^{m}\left[\frac{3\cdot c_{pj}}{v_{dc}}\frac{\mathrm{d}}{\mathrm{d}t}w_j + \frac{p_{acj}^*}{v_{dc}} - \frac{1}{\rho_j}\left(\frac{v_{dc}^*}{v_{dc}} - 1\right)\right] \quad (10)$$

Equation (10) captures the relation between the dc voltage, the arm energy, and the ac active power. For example, in the case where terminal j is providing POD service, the oscillating power Δp_{acj} will be added to p_{acj}^*. The effect of Δp_{acj} can be locally compensated for at terminal j by setting the energy reference as given in (11).

$$\Delta w_j^* = -\frac{1}{3c_{pj}}\int \Delta p_{acj}\,\mathrm{d}t \quad (11)$$

Substituting (11) in (10), it can be seen that the effect of Δp_{acj} can be canceled and the oscillation does not appear in the dc voltage. This was the approach followed in [6]. However, as mentioned in the introduction, the amount of power available from one converter is limited and hence, contribution from other converters might be required for effective reduction of a disturbance. Such an arrangement requires that the active power deviation be communicated to all terminals participating in the service, which is impractical. Therefore, an alternative approach is considered here. Instead of canceling the effect of the disturbances, the proposed method works on strengthening the dc grid by increasing the effective dc capacitance.

Ref. [11] presents one such approach where the arm energy reference is varied proportional to the stored energy in the dc grid. This virtually connects the arm capacitance in parallel with the grid capacitance. This approach will be referred to as Fixed Capacitance Support (FCS) henceforth since it increases the grid capacitance by a fixed amount. The per-unit implementation of this approach is given by (12) where
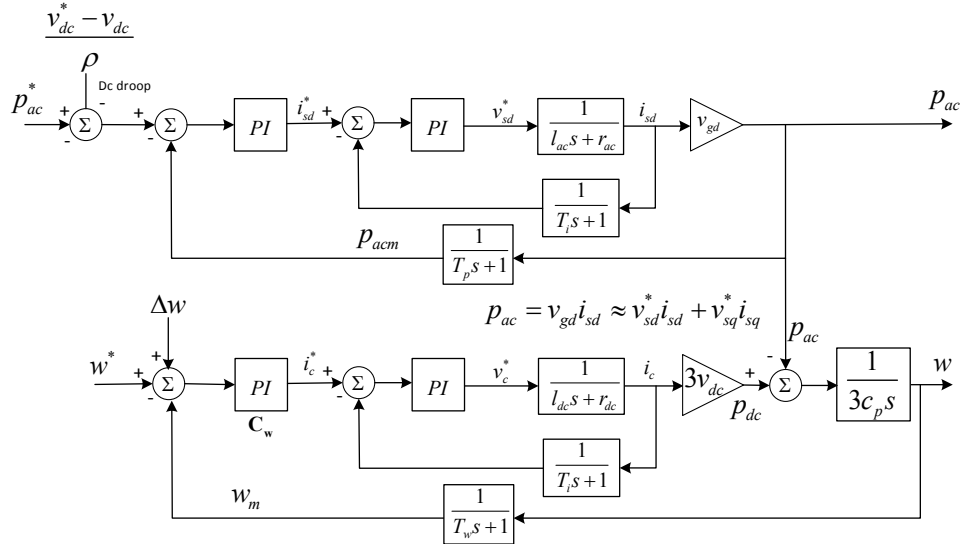
Figure 2: MMC controller block diagram.

k is a control parameter deciding the amount of additional capacitance obtained.

$$w_j^* = k_j \cdot v_{dc}^2 = w_j \tag{12}$$

$$\frac{\mathrm{d}}{\mathrm{d}t} w_j = 2 \cdot k_j \cdot v_{dc} \frac{\mathrm{d}}{\mathrm{d}t} v_{dc} \tag{13}$$

After substituting (13) in (8) and rearranging the terms, (14) is obtained.

$$c_{eq} \frac{\mathrm{d}}{\mathrm{d}t} v_{dc} = -\sum_{j=1}^{m} \left[\frac{p_{acj}^*}{v_{dc}} - \frac{1}{\rho_j} \left(\frac{v_{dc}^*}{v_{dc}} - 1 \right) \right] \tag{14}$$

$$where \quad c_{eq} = c_g + \sum_{j=1}^{m} 6 \cdot k_j \cdot c_{pj}$$

From (14), one can see that the grid capacitance is effectively increased. Each MMC contributes by inserting 6 of its arm capacitors scaled by the respective k_j. In order to evaluate the method, (14) is linearized around an operating point where the sum of active power references, p_{acj}^* is 0 and $v_{dc}^* = v_{dc} = v_{dc0}$.

$$c_{eq} \frac{\mathrm{d}}{\mathrm{d}t} \Delta v_{dc} = -\sum_{j=1}^{m} \frac{\Delta p_{acj}^*}{v_{dc0}} - \sum_{j=1}^{m} \frac{\Delta v_{dc}}{\rho_j v_{dc0}} \tag{15}$$

Each signal is prefixed with a Δ to indicate a small deviation around the operating point. Applying Laplace transform and rearranging the terms in (15), the transfer function from Δp_{acj} to Δv_{dc} can be calculated as given in (16).

$$\Delta v_{dc} = -\frac{\rho_{eq}}{T_{eq} s + 1} \sum_{j=1}^{m} \Delta p_{acj}^* \tag{16}$$

$$where \quad \rho_{eq} = \left(\sum_{j=1}^{m} \frac{1}{\rho_j} \right)^{-1} \quad and \quad T_{eq} = c_{eq} \cdot \rho_{eq} \cdot v_{dc0}$$

Equation (16) indicates that any disturbance in the active power passes through an equivalent low-pass filter with time-constant T_{eq} before appearing on the dc voltage. Therefore, a large value of T_{eq} (in the order of seconds) is desirable in order to get good attenuation in the frequency range of interest. For example, to get more than a factor 5 attenuation at $1\,\mathrm{Hz}$, T_{eq} has to be greater than $800\,\mathrm{ms}$. This requires the gains k_j to be in the order of hundreds since the capacitances, in pu, are in the order of few tens of milliseconds and ρ_{eq} is in the order of few percent. However, the average arm voltage will be equal to $\sqrt{k} \times v_{dc}$. This fact restricts the value of k to be close to 1 which makes the FCS ineffective for this application. The next section discusses an alternative approach which offers better performance.

IV. PROPOSED SCHEME

The main limitation of the FCS scheme is that the gain has to be close to 1. This can be avoided by applying the amplification to the deviation in dc voltage, Δv_{dcf}, over a desired frequency range ($0.2\,\mathrm{Hz}$ to $2\,\mathrm{Hz}$) instead of the complete signal. The energy reference is then modified as shown in (17).

$$w_j^* = w_0 + k_j \cdot \Delta v_{dcf}^2 \tag{17}$$

where w_0 is a reference related to the average arm voltage, which is constrained such that the arm voltage is close to v_{dc}. The scheme creates the same effect as the FCS, but now there is less restriction on the gain. It provides capacitance support only during transients over a desired frequency range. Therefore, it will be referred to as Dynamic Capacitance Support (DCS). This method requires separation of the desired frequency components, Δv_{dcf}, from the measured signal, v_{dc}. This can be achieved by using the proposed scheme shown in Fig. 3. The first stage is a washout filter to remove the dc components followed by a low-pass filter to limit the gain at high frequencies. The overall transfer function resembles a bandpass filter. It is important to have low phase shift in the pass band. Therefore, the filters are designed to give zero phase shift at $1\,\mathrm{Hz}$ i.e. the middle of the desired interval. Further phase adjustment can be made by using lead-lag filters.

The upper limit on the gain is due to the output saturation in Fig. 3. Once the output saturates, the converter immediately stops providing the capacitance supports. This is because the current injection is proportional to the derivative of the stored energy, (see (8)). Since the stored energy is related to the arm voltage ($w = v^2$), the limits are coupled to the design of the converter. The upper limit is defined by the maximum voltage at which the arms can be operated, which is, in turn, defined by the maximum continuous sub-module voltage rating. The lower limit, on the other hand, is constrained by the lowest possible arm voltage without causing over-modulation. Over-modulation occurs when the reference inserted voltage is greater than the sum of capacitor voltages. In order to accommodate downward changes in the stored energy without causing over-modulation, the arm voltage should be operated with a headroom above the dc voltage. The MMC is normally designed such that the average arm voltage equals the dc voltage. Therefore, the headroom requires either additional sub-modules or operation of each-module at a higher voltage. The first option can be more attractive in some cases because most MMCs are equipped with redundant sub-modules. However, as the number of modules increases, the capacitance decreases because of the series connection. So, the second option offers a higher gain for the same percentage increase [6]. For the purpose of this paper, the second option is adopted with the sub-module voltage increased by $15\,\%$. This corresponds to the gain for the FCSs being set to $k_j = 1.15^2 = 1.31$. The DCSs, on the other hand, will be simulated with different gain values with the default being 100.
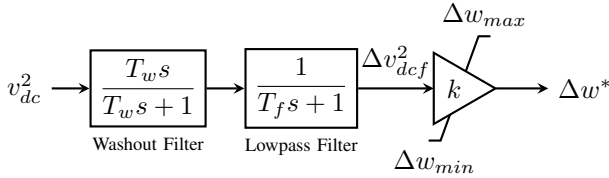

Figure 3: Dynamic Capacitance Support (DCS) block.

V. SIMULATION RESULTS

Simulation results under different cases will be presented in this section. First, the test system will be described, followed by simulation results for two case studies: active power reference change, and POD.

A. The Test System

The system used to test the proposed scheme is a four terminal dc grid [12] shown in Fig. 4. There are two offshore wind farms connected to converters 1 and 2. The other two converters are connected to two independent onshore ac grids. All the converters are MMCs with parameters given in Table II. The wind farm converters are controlled in power mode so they do not participate in dc voltage control. The remaining converters are controlled in dc-droop mode with a droop value of $10\,\%$. In the base case, the wind farms connected to converters 1 and 2 are injecting $300\,\text{MW}$ and

TABLE II: Converter Parameters [12]

Parameter	Converters 1, 2, and 3	Converter 4
Base apparent power, S_b	$900\,\text{MVA}$	$1200\,\text{MVA}$
Base dc voltage, V_b^{dc}	$640\,\text{kV}$	$640\,\text{kV}$
AC Frequency, f	$50\,\text{Hz}$	$50\,\text{Hz}$
Arm capacitance, C_{arm}	$29.3\,\mu\text{F}$	$39\,\mu\text{F}$
Arm inductance, L_{arm}	$84.8\,\text{mH}$	$63.6\,\text{mH}$
Arm resistance, R_{arm}	$0.885\,\Omega$	$0.67\,\Omega$
Transformer reactance, X_t	$17.7\,\Omega$	$13.4\,\Omega$
Transformer resistance, R_t	$1.77\,\Omega$	$1.34\,\Omega$

$800\,\text{MW}$, respectively. Converters 3 and 4 share the total power injection according to their droop settings and rated powers. The sign convention is such that active power injected by the wind farms is positive while absorption is positive for the onshore ac grids. The total dc grid capacitance was calculated to be ≈ 0.075 pu which leads to $T_{eq} \approx 17\,\text{ms}$ with $\rho_{eq} = 4.3\,\%$. The washout and low-pass filter time-constants are $0.25\,\text{s}$ and $0.1\,\text{s}$, respectively.
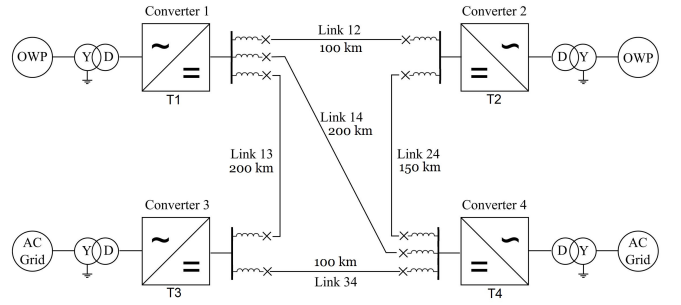

Figure 4: Test grid used for simulation [12]

B. Active power reference change

The purpose of this case study is to show the response of the system to power reference changes without (Base case) and with the proposed controller. For this purpose, two reference changes are introduced. First, power injection from converter 2 is reduced from $800\,\text{MW}$ to $720\,\text{MW}$ at $t = 2\,\text{s}$. This process is rate-limited by applying a first-order low-pass filter with time-constant of $750\,\text{ms}$ on the reference power. Then at $t = 15\,\text{s}$, the output power of converter 1 is abruptly dropped from $300\,\text{MW}$ to $0\,\text{MW}$ in order to simulate a sudden loss of generation from the wind farm. Fig. 5 shows the ac active power at each of the converters. The corresponding dc voltages
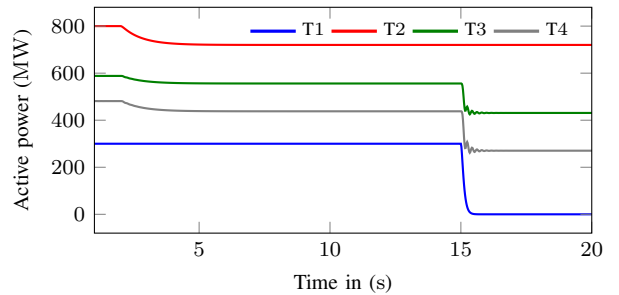
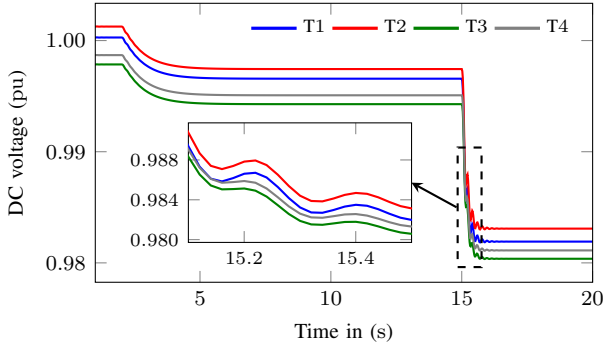

Figure 5: Base case ac powers.
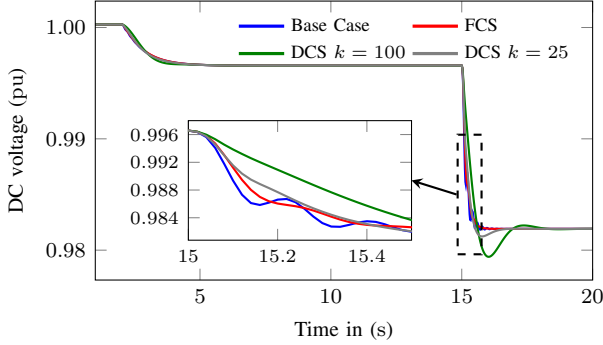
Figure 6: Base case dc voltages.
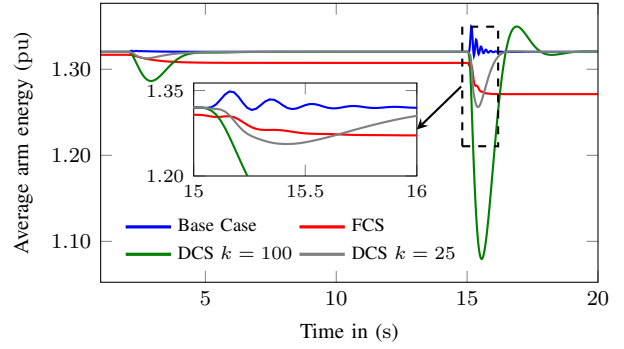

Figure 8: Arm energy of T1 with capacitance support.

Figure 7: DC voltage of T1 with capacitance support.

Figure 9: POD Active power without and with capacitance support, $k = 100$.

are displayed in Fig. 6. Both results show a smooth transition for the first change but a small oscillation is observed for the case of the abrupt change at $t = 15\,\mathrm{s}$. The oscillation is due to the presence of an under-damped mode in the system. It can also be noted that the wind farm converters do not participate in dc voltage control so their active power is independent of the dc voltage. After the abrupt change, converters 3 and 4 reduce their active power absorption and converter 4 takes a larger share because of its larger rating. Since the dc voltages have similar features, only the voltage at converter 1 will be displayed in subsequent results. Figs. 7 and 8 show the dc voltages and stored energy when the capacitor support schemes are enabled. It can be seen that for the FCS case, the dc voltage exhibits negligible oscillation. This is because the rate of change of dc voltage is reduced by the filtering effect of the FCS. The DCS shows no oscillation but there is a large undershoot in the voltage because the DCS approach behaves like a second-order low-pass filter with a complex pole-pair and a higher gain results in lower damping. When the gain is reduced to 25, the undershoot reduces significantly, (Fig. 7). The gain reduction also leads to a lower energy deviation, (Fig. 8).

C. Power Oscillation Damping (POD)

This section presents a case study where converter 3 is providing POD to the connected onshore ac grid. The POD action is emulated by adding a $1\,\mathrm{Hz}$ damped oscillation with damping of $5\,\%$ and magnitude of $70\,\mathrm{MW}$ to the active power reference of converter 3 at $t = 7\,\mathrm{s}$. Active powers are displayed

in Fig. 9 where it can be observed that the active power of converter 3 exhibits oscillating power of maximum magnitude approximately $30\,\mathrm{MW}$. This magnitude is lower than the reference because of the droop action. This power oscillation causes the dc voltage to oscillate, which is then picked-up by any terminal participating in dc voltage control. Thus, a comparable magnitude oscillation is seen in the active power of converter 4. The dc voltage at converter 1 is shown in Fig. 10 for three different cases. The Base Case is without any capacitance support. It can be noted that the voltage deviations are very small even in the base case. This is because the other ac grid, i.e. converter 4, is injecting the required POD power quickly such that the dc grid capacitance does not have to source a large current. When FCS is applied to all terminals, the oscillation in dc voltage shows negligible change. The proposed scheme (DCS) on the other hand, is able to show significant improvement because the gain is much larger, (Fig. 10). Increasing the gain further results in close to ideal performance but as indicated in the previous section higher gain results in overshoot. Hence, further small signal analysis is needed for selecting the most appropriate gain. However, the main goal is to divert the power distortions into the arm capacitors, which can be seen from Figs. 9 and 11. It is evident that propagation of the oscillation is reduced when the DCS scheme is enabled. Moreover, the POD power from converter 3 exhibits an increase in magnitude. This can be attributed to the droop action, which tries to reduce Δv_{dc}
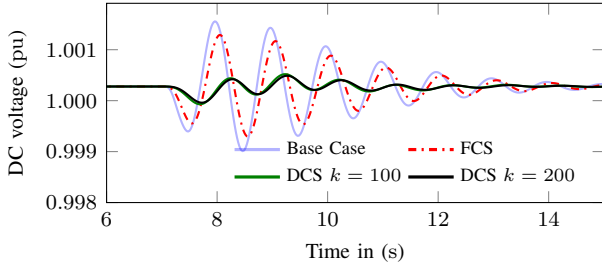
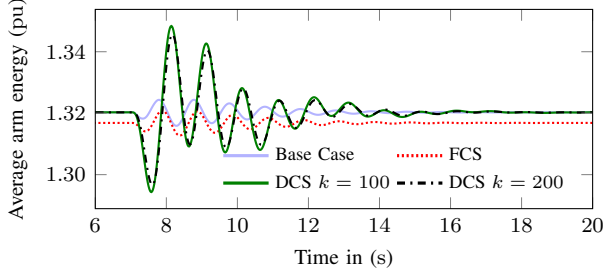Figure 10: DC voltages with capacitance support, POD.

Figure 11: Arm energy with capacitance support, POD.

voltage by opposing the change in active power. But, with the DCS scheme, the dc link will be stiffer, which means that Δv_{dc} is lower for the same Δp_{ac}. Hence, the reduction in power reference due to the droop action will be lower.

VI. CONCLUSION

This paper proposes a control scheme that will increase stiffness of the dc grid over a specific frequency range to reduce the impact of active power disturbance related to ancillary services. Although the main focus has been Power Oscillation Damping (POD), the method can be extended to other services related to active power. Each converter only uses local dc voltage measurement making it an inherently distributed approach. Thus, extension to larger systems is straightforward. The approach is compared to the FCS scheme where the stored arm energy is controlled to emulate an extra capacitance connected to the dc grid. The main limitation of FCS is that the gain is constrained to be close to 1 and thus, cannot provide noticeable support in the application of interest. The proposed approach (Dynamic Capacitance Support) overcomes this constraint by applying amplification of the voltage deviation over a desired frequency range. This was demonstrated by simulation results where it was shown that the active power distortions are effectively diverted in to the arm capacitors. The dc voltage is used as a means of communicating the distortions to all the terminals. It was also noted that with higher gain the DCS scheme performs better. However, as the gain increases, the risk of saturation also increases. When the DCS output is saturated, the converter will immediately stop providing capacitance support which is undesirable. Thus, the gain should be calculated based on the amount of available storage capacity and expected level of disturbance in terms of magnitude and frequency. The

largest energy deviation is observed in the case of abrupt change in active power. This was also accompanied by a large undershoot in dc voltage which was improved by reducing the gain. This contrasts with the high gain requirement of the POD. Therefore, the choice depends on the intended use of the storage capacity. For example, if the main goal is to provide POD, the gain can be large without causing significant deviations in the arm energy, ($<5\%$). This would also entail lower storage capacity requirement.

APPENDIX

The base values used for per-unit calculations are depicted in (18). The base dc voltage is $640\,\text{kV}$ and the system power base is $900\,\text{MVA}$.

$$I_b^{ac} = \frac{2}{3}\frac{S_b}{V_b^{ac}} \quad Z_b^{ac} = \frac{V_b^{ac}}{I_b^{ac}} \quad I_b^{dc} = \frac{S_b}{V_b^{dc}} \quad Z_b^{dc} = \frac{V_b^{dc}}{I_b^{dc}}$$

$$L_b^{ac} = Z_b^{ac} \quad C_b^{ac} = \frac{1}{Z_b^{ac}} \quad L_b^{dc} = Z_b^{dc} \quad C_b^{dc} = \frac{1}{Z_b^{dc}}$$

$$V_b^{dc} = 2V_b^{ac} \qquad W_b = \frac{1}{2}C_{arm}\left(V_b^{dc}\right)^2 \qquad (18)$$

REFERENCES

[1] "Establishing a network code on requirements for grid connection of high voltage direct current systems and direct current-connected power park modules," *Commission Regulation (EU) 2016/ 1447*, vol. 59, no. L 241, Aug. 2016.
[2] T. M. Haileselassie, R. E. Torres-Olguin, T. K. Vrana, K. Uhlen, and T. Undeland, "Main grid frequency support strategy for VSC-HVDC connected wind farms with variable speed wind turbines," in *2011 IEEE Trondheim PowerTech*, Jun. 2011, pp. 1–6.
[3] L. Harnefors, N. Johansson, L. Zhang, and B. Berggren, "Interarea oscillation damping using active-power modulation of multiterminal HVDC transmissions," *IEEE Transactions on Power Systems*, vol. 29, no. 5, pp. 2529–2538, 2014.
[4] A. G. Endegnanew, "Stability Analysis of High Voltage Hybrid AC/DC Power Systems," PhD Dissertation, NTNU, Trondheim, Norway, 2017.
[5] C. D. Barker, R. S. Whitehouse, A. G. Adamczyk, and G. G. Soto, "Low frequency active power oscillation damping using a MMC-VSC HVDC link," in *13th IET International Conference on AC and DC Power Transmission (ACDC 2017)*, Feb. 2017, pp. 1–6.
[6] A. A. Taffese, E. Tedeschi, and E. de Jong, "A control scheme for utilizing energy storage of the modular multilevel converter for power oscillation damping," in *2017 IEEE 18th Workshop on Control and Modeling for Power Electronics (COMPEL)*, Jul. 2017, pp. 1–8.
[7] G. Bergna Diaz, J. A. Suul, and S. D'Arco, "Small-signal state-space modeling of modular multilevel converters for system stability analysis," in *Energy Conversion Congress and Exposition (ECCE), 2015 IEEE*. IEEE, 2015, pp. 5822–5829.
[8] A. A. Taffese, E. Tedeschi, and E. de Jong, "Arm voltage estimation method for compensated modulation of modular multilevel converters," in *2017 IEEE Manchester PowerTech*, Jun. 2017, pp. 1–6.
[9] K. Sharifabadi, L. Harnefors, H.-P. Nee, S. Norrga, and R. Teodorescu, *Design, Control and Application of Modular Multilevel Converters for HVDC Transmission Systems*. Chichester, UK: John Wiley & Sons, Ltd, Aug. 2016.
[10] J. W. Umland and M. Safiuddin, "Magnitude and symmetric optimum criterion for the design of linear control systems: What is it and how does it compare with the others?" *IEEE Transactions on Industry Applications*, vol. 26, no. 3, pp. 489–497, May 1990.
[11] S. Samimi, F. Gruson, P. Delarue, F. Colas, M. M. Belhaouane, and X. Guillaud, "MMC Stored Energy Participation to the DC Bus Voltage Control in an HVDC Link," *IEEE Transactions on Power Delivery*, vol. 31, no. 4, pp. 1710–1718, Aug. 2016.
[12] W. Leterme, N. Ahmed, J. Beerten, L. Angquist, D. V. Hertem, and S. Norrga, "A new HVDC grid test system for HVDC grid dynamics and protection studies in EMT-type software," in *11th IET International Conference on AC and DC Power Transmission*, Feb. 2015, pp. 1–7.